



## Article

# Spontaneous Adsorption and Efficient Photodegradation of Indigo Carmine under Visible Light by Bismuth Oxyiodide Nanoparticles Fabricated Entirely at Room Temperature

Mohamed R. Elamin <sup>1</sup>, Khalid H. Ibnaouf <sup>2</sup> , Nuha Y. Elamin <sup>1</sup>, Fatima A. Adam <sup>1</sup>, Abdulrahman H. Alolayan <sup>1</sup> and Babiker Y. Abdulkhair <sup>1,\*</sup>

<sup>1</sup> Chemistry Department, College of Science, Imam Mohammad Ibn Saud Islamic University (IMSIU), Riyadh 11623, Saudi Arabia; mrabuzaid@imamu.edu.sa (M.R.E.); nyelamin@imamu.edu.sa (N.Y.E.); famohamedali@imamu.edu.sa (F.A.A.); aholyan@imamu.edu.sa (A.H.A.)

<sup>2</sup> Physics Department, College of Science, Imam Mohammad Ibn Saud Islamic University (IMSIU), Riyadh 13318, Saudi Arabia; khiahmed@imamu.edu.sa

\* Correspondence: byabdulkhair@imamu.edu.sa or babbiker35.by@gmail.com

**Abstract:** Bismuth oxyiodide (BiOI) is a targeted material for its relative safety and photocatalytic activity under visible light. In this study, a successful simple and energy-saving route was applied to prepare BiOI through a sonochemical process at room temperature. The characterization of the prepared BiOI was conducted by physical means. The transmission electron microscope (TEM) image showed that the BiOI comprises nanoparticles of about 20 nm. Also, the surface area of the BiOI was found to be  $34.03 \text{ m}^2 \text{ g}^{-1}$  with an energy gap of 1.835 eV. The adsorption and photocatalytic capacities of the BiOI were examined for the indigo carmine dye (IC) as a model water-pollutant via the batch experiment methodology. The solution parameters were optimized, including pH, contact time, IC concentration, and temperature. Worth mentioning that an adsorption capacity of  $185 \text{ mg.g}^{-1}$  was obtained from  $100 \text{ mg L}^{-1}$  IC solution at  $25^\circ\text{C}$  within 60 min as an equilibrium time. In addition, the BiOI showed a high degradation efficiency towards IC under tungsten lamp (80 W), where 93% was removed within 180 min, and the complete degradation was accomplished in 240 min. The fabricated BiOI nanoparticles completely mineralized the IC under artificial visible light, as indicated by the total organic carbon analysis.

**Keywords:** bismuth oxyiodide; sonochemical synthesis; indigo carmine; adsorption; visible-light photodegradation



**Citation:** Elamin, M.R.; Ibnaouf, K.H.; Elamin, N.Y.; Adam, F.A.; Alolayan, A.H.; Abdulkhair, B.Y. Spontaneous Adsorption and Efficient Photodegradation of Indigo Carmine under Visible Light by Bismuth Oxyiodide Nanoparticles Fabricated Entirely at Room Temperature. *Inorganics* **2022**, *10*, 65. <https://doi.org/10.3390/inorganics10050065>

Academic Editor: Antonino Gulino

Received: 12 April 2022

Accepted: 17 May 2022

Published: 19 May 2022

**Publisher's Note:** MDPI stays neutral with regard to jurisdictional claims in published maps and institutional affiliations.



**Copyright:** © 2022 by the authors. Licensee MDPI, Basel, Switzerland. This article is an open access article distributed under the terms and conditions of the Creative Commons Attribution (CC BY) license (<https://creativecommons.org/licenses/by/4.0/>).

## 1. Introduction

The deterioration of natural water resources by synthetic organic compounds is a significant challenge facing the globe. Wastewater from different anthropological activities transports the residues of the organic contaminants to the natural water resources. Synthetic organic dyes are considered high oxygen demanding substances that consume a considerable amount of the oxygen in water, causing severe damage to aquatic life [1,2]. In addition, the turbidity caused by the coloring dyes and suspensions reduce the light penetration, decreasing the photosynthesis efficiency of the algae and breaking the food cycle in the aquatic ecosystems [3]. Many physical, chemical and biological methods were employed to remove pollutants from water and wastewater, including oxidation, solvent extraction, biodegradation, membrane process, and adsorption, all practiced alone or combined [4–6].

Adsorption and photodegradation are among the most applied water treatment methods due to their simplicity and excellent efficiency [7,8]. An ongoing research trend is the innovation of efficient and multifunctional materials for water treatment. Various substances were recently tested for their adsorption, photocatalytic, and disinfectant properties on the condition of being environmentally friendly substances. Some nanomaterials

possessed adsorption and photocatalysis activities, such as zinc oxide and titanium dioxide. [9,10]. Most prepared materials utilize the relatively expensive and harmful ultraviolet radiation (UV). In order to avoid the carcinogenic effects of UV light, the synthesis of photocatalysts to oxidize organic pollutants under visible light is a recent trend. Hence, bismuth-based nanomaterials (BiOI, BiOBr, and BiOCl) have been targeted [11–13]. The photochemical properties of bismuth oxyiodide (BiOI) make it an excellent candidate for degrading organic pollutants in water [14,15]. The low bandgap-energy (ca 1.8 eV) of bismuth oxyiodide, relative safety, and cost motivate researchers to innovate many synthesis routes. Scientists continuously seek a quick, safe, and economic methodology for preparing BiOI. Almost 400 papers have been issued about fabricating or utilizing BiOI with various energy and time-consuming methods in the last twelve years. BiOI was synthesized using water or organic solvents via hydrothermal or solvothermal techniques [16–19]. A recent study prepared BiOI nanoflakes via some routes starting at room temperature and then followed by autoclave incubation [20]. To the best of our knowledge, none of the methods prepared BiOI nanoparticles entirely at room temperature.

This study hypothesized that the energy and time-consuming incubation step could be eliminated by synthesizing BiOI entirely at room temperature through a sonochemical method. The product obtained will be characterized and applied to remove indigo carmine (IC) dye as a model organic pollutant via adsorption and photodegradation under artificial visible light.

## 2. Experimental

### 2.1. Materials

Potassium iodide (KI) and bismuth nitrate pentahydrate ( $\text{Bi}(\text{NO}_3)_3 \cdot 5\text{H}_2\text{O}$ ) were provided from BDH-England. The ethylene glycol was supplied from Sharlau-Spain, and the indigo carmine dye was from Fisher Scientific (Loughborough, UK).

### 2.2. Sonochemical Preparation of BiOI Nanoparticles

9.70 g of  $\text{Bi}(\text{NO}_3)_3 \cdot 5\text{H}_2\text{O}$  was dispersed in 200 mL tri-ethylene glycol. 3.32 g of KI were dispersed in 50 mL tri-ethylene glycol. The KI solution was added in small portions to the bismuth nitrate solution in a temperature-controlled ultrasonic bath (Labtech-LTUSB, Korea) adjusted to 25 °C. Following 20 min of sonication, the mixture was poured into 500 mL of distilled water and continuously shaken for 10 min (25 °C). The product was filtered, washed with distilled water, and dried at 105 °C for three hours.

### 2.3. Characterization of BiOI Nanoparticles

The prepared BiOI was analyzed utilizing a powder X-ray diffractometer (D8 Advance, Bruker, Billerica, MA, USA), scanning electron microscopy (SEM)-JSM-IT300, transmission electron microscopy (TEM-100 kV), surface analyzer (ASAP 2020 micromeritics, USA). Fourier transform infrared spectroscopy (FTIR, Bruker TENSOR Series, Germany) was used to analyze the KBr: sample disk of 20:1 ratio. The diffuse reflectance spectrum of BiOI was recorded using  $\text{BaSO}_4$  as a reference by the Shimadzu Uv-vis spectrophotometer (2600i Uv-vis, Japan).

### 2.4. Adsorption of IC by BiOI

The solution parameters for IC sorption on BiOI were studied. 240 mL of  $20 \text{ mg L}^{-1}$  of IC solution and 100 mg of the prepared BiOI were stirred together for the kinetic investigations. An aliquot of the mixture was withdrawn each interval of time, filtered, and absorbance was measured until equilibrium. Further, the optimum pH for the adsorption was examined within the pH range of 3 to 9. The pH effect on the color of the IC was considered, so the standard solution ( $20 \text{ mg L}^{-1}$ ) was adjusted to the same sample pH before comparing their absorbance. 10, 20, 50, and  $100 \text{ mg L}^{-1}$  of IC solutions were employed to inspect the concentration's influence on sorption by BiOI. In addition, the temperature impact on the sorption process was examined at 20 °C, 35 °C, and 50 °C using the same concentrations.

## 2.5. Photodegradation of IC by BiOI

The synthesized BiOI was tested for photodegrading IC in synthetic polluted water. The process was conducted by mixing 50 mg of BiOI with 200 mL of 20 mg L<sup>-1</sup> IC-solution. The mixture was stirred for 2 h in darkness, then placed under tungsten lamp (80 Watt) [21]. The remaining concentration of IC was monitored using a UV-VIS-spectrophotometer. Additionally, the total organic carbon (TOC) results of the filtered sample and that with the BiOI suspension were used to propose the mechanism of IC degradation.

## 3. Results and Discussion

### 3.1. Characterization

Figure 1 revealed the surficial structure of the synthesized BiOI being explored by SEM. The BiOI presented a nanosheet structure with a 27.0 to 48.0 nm thickness range. In addition, the elemental composition of the sonochemically-prepared BiOI was carried out using EDX. The obtained results (Figure 2a) showed that the prepared material was composed of bismuth, iodide, and oxygen at 58.1%, 6.1%, and 33.8%, respectively. These practical results are consistent with the theoretical composition of BiOI, the bit of variation can be attributed to adsorbed-moisture revealed in the FT-IR results. In addition, the elemental mapping monitored in Figure 2b–d indicated an excellent homogeneity for the Bi, O, and I elements. Further, the fabricated BiOI nanosheet's detailed morphology was examined using TEM. Figure 3a showed clusters of particles ranging between 85 to 190 nm, and these clusters are composed of smaller nanoparticles in the range of 5 to 10 nm (Figure 3b). This fast method yields smaller particles than more sophisticated and energy-consuming methods [22–25].

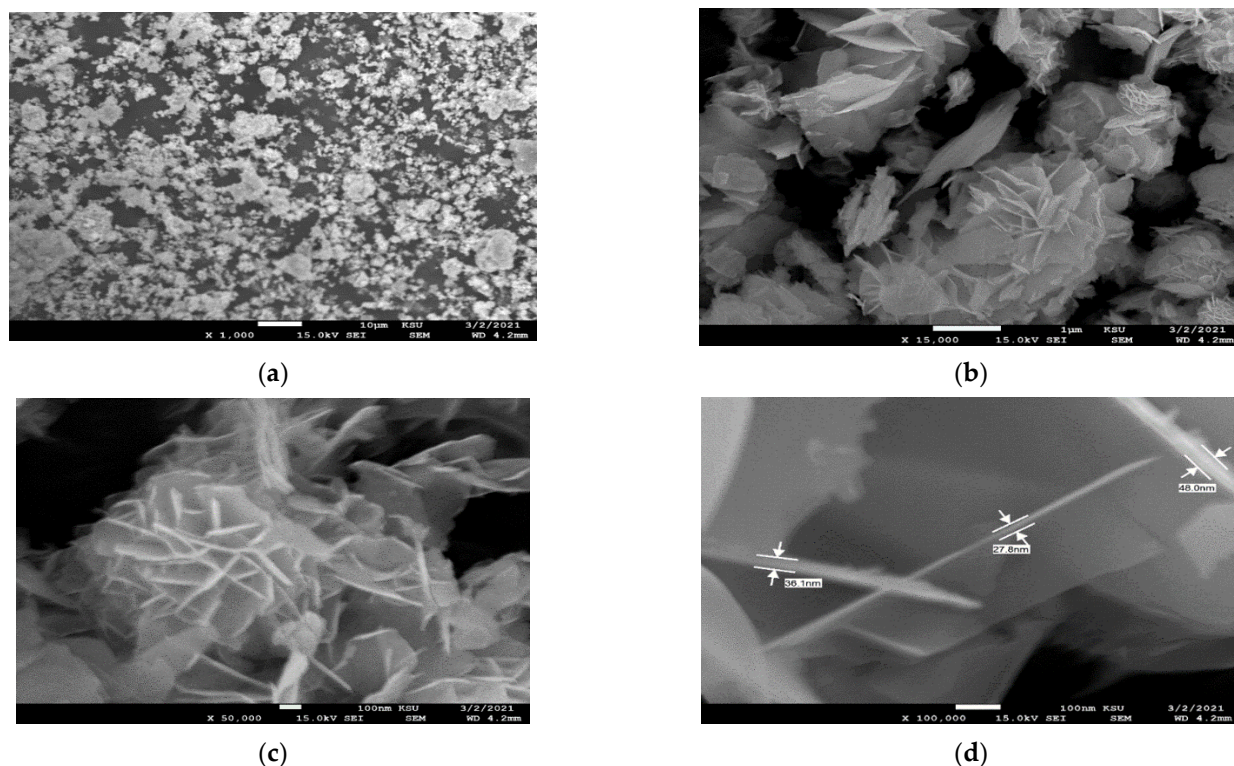


**Figure 1.** (a–d) The SEM results for the BiOI nanosheets synthesized by sonochemical method at room temperature.

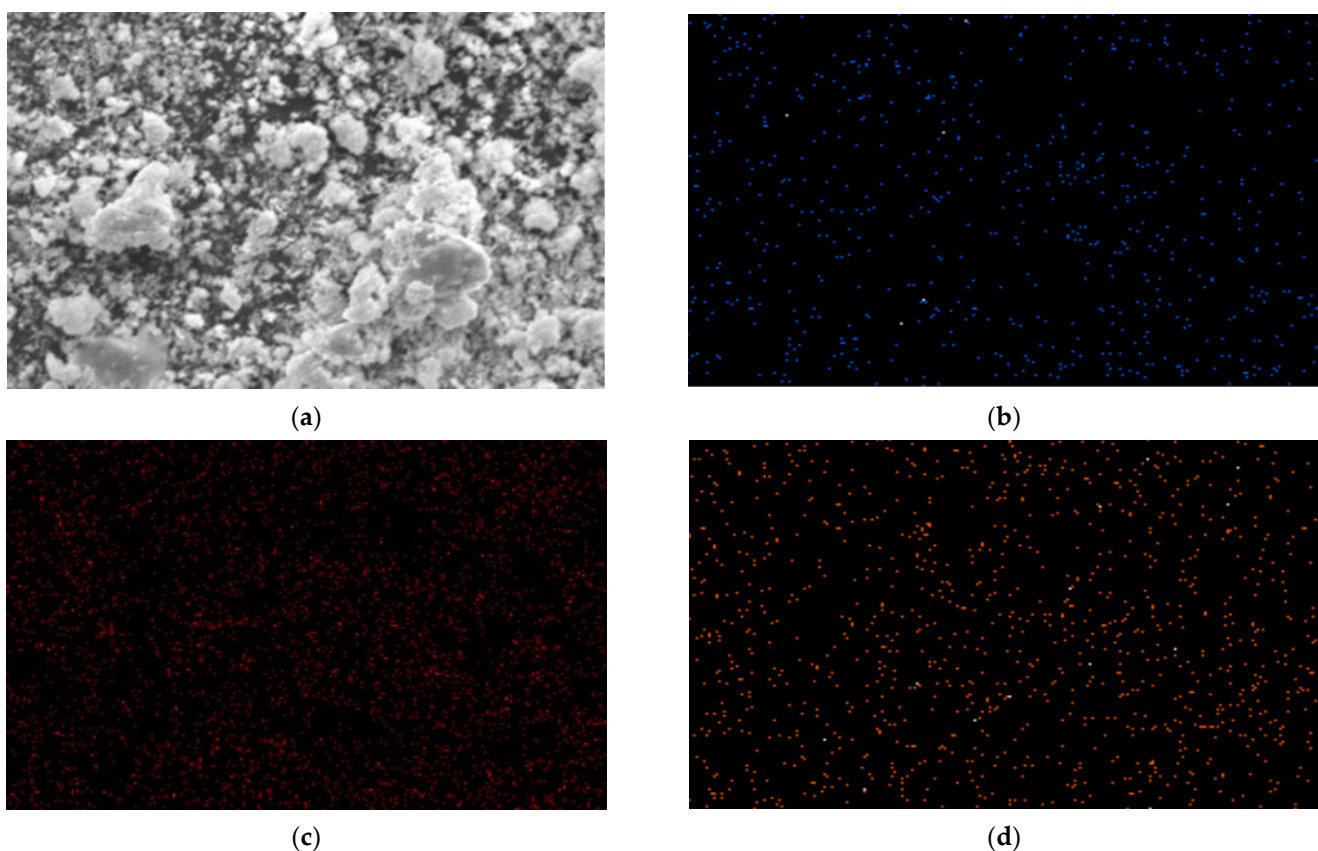


**Figure 2.** (a) EDX results for the BiOI nanosheets synthesized by sonochemical method at room temperature; (b–d) elemental mapping of oxygen, Iodide, and bismuth in the prepared BiOI.

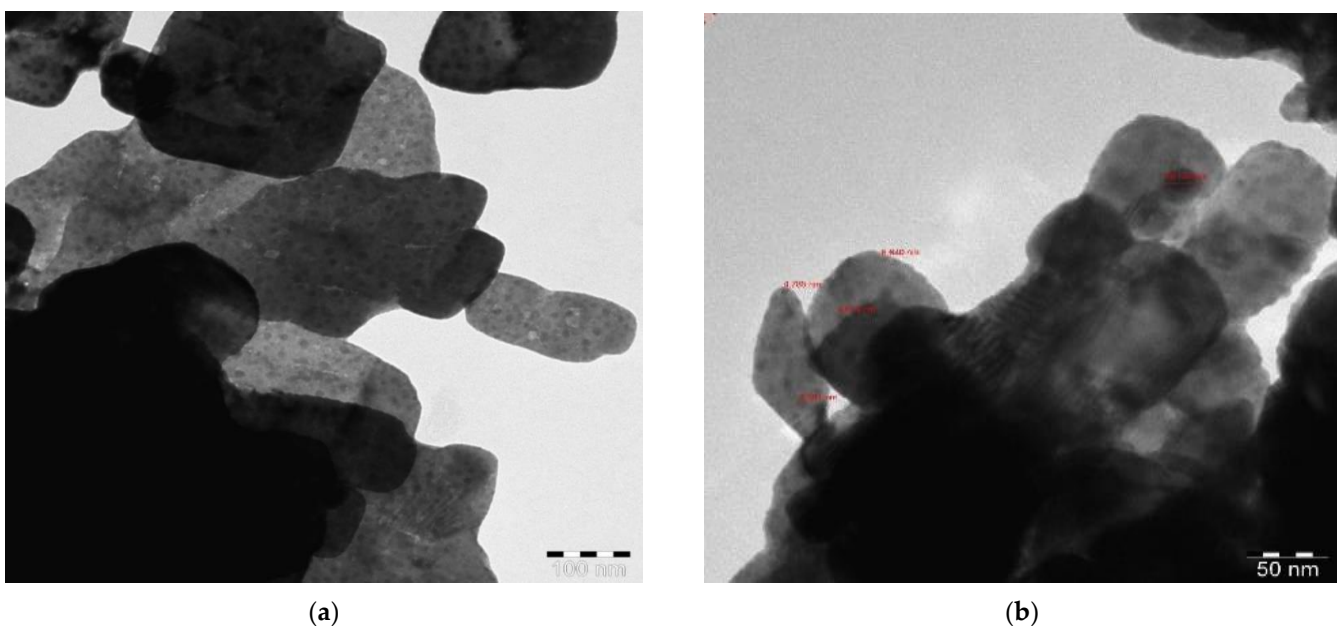


**Figure 3.** (a,b) The TEM results for the BiOI nanoparticles synthesized by sonochemical method at room temperature.

The XRD was utilized to examine the crystallography of the as-synthesized BiOI. The resulting diffraction pattern in Figure 4a corresponds to the BiOI-tetragonal lattice structure (JCPDS 00-010-0445) [26]. The sharp and intense peaks at  $2\theta^\circ$  of 29.6 and 31.6 indicated good crystallinity for this product. These findings suggested an efficient performance for

the prepared BiOI concerning the charge separation and transfer during the photodegradation [27]. Furthermore, Bragg's angle was employed in determining the crystal size via Debye–Scherer's relation expressed by Equation (1).

$$D = \frac{k \cdot \lambda}{\beta \cos \theta} \quad (1)$$

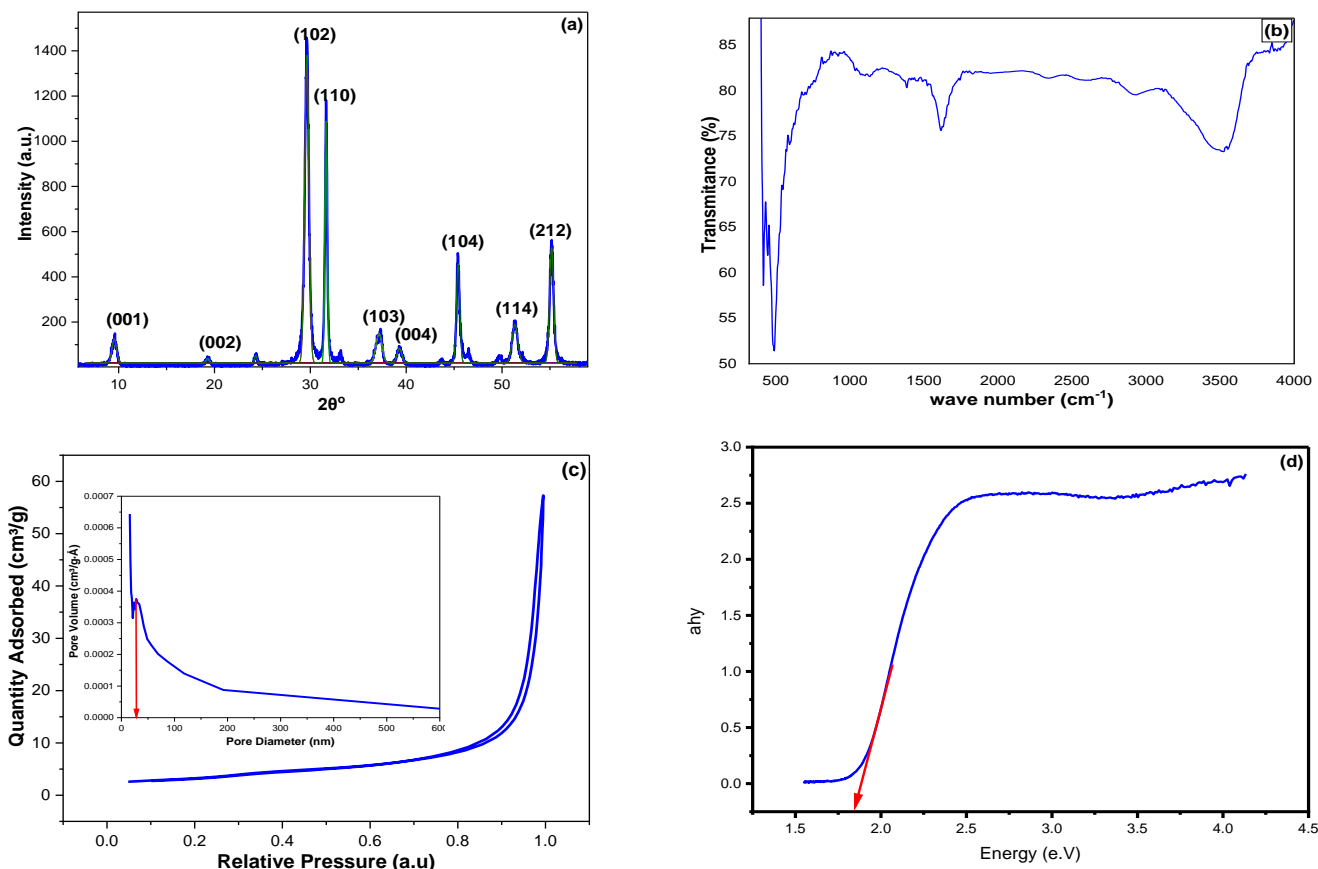


**Figure 4.** (a) XRD pattern for the synthesized BiOI nanoparticles; (b) the FT-IR vibration bands for the prepared BiOI nanoparticles; (c) the surface characteristics for the synthesized BiOI nanoparticles; (d) the energy-band-gap for the fabricated BiOI nanoparticles.

D,  $\lambda$ , and  $\beta$  represent the average crystal size, radiation wavelength, and peak width at its half-maximum.

The average crystal size for the room temperature-synthesized BiOI was about 17 nm by all peaks included in the calculation, while 15 nm crystal size was obtained when the principal peak at  $2\theta^\circ$  of 29.6 was employed. The XRD average crystals size of 17 nm agreed with the TEM results since the ultrasmall particles were amorphous, and the diffraction peaks resulted from the larger ones, which were crystalline.

Figure 4b monitored the FTIR results for the sonochemically synthesized BiOI. The vibration peaks between  $400 \text{ cm}^{-1}$  to  $850 \text{ cm}^{-1}$  correspond to the Bi–I, O–I, and Bi–O bonds. The broadband between  $3200 \text{ cm}^{-1}$  to  $3500 \text{ cm}^{-1}$  refers to an O–H of adsorbed moisture [28,29]. Worth mentioning that the prevalence of water molecules on the BiOI via the FT-IR may justify the minor increase of oxygen within the EDX results.

The surface area (SA), pore diameter (PD), and pore volume (PV) of the synthesized BiOI were determined via the  $N_2$  adsorption-desorption method. Figure 4c revealed that BiOI exhibited a hysteresis loop of type (III) distinctive for a non-rigid-platelike aggregate with cylindrical macropores [18,30–36]. The obtained SA, PD, and PV values for the BiOI were  $34.03 \text{ m}^2 \cdot \text{g}^{-1}$ , 1.579 nm, and  $0.054 \text{ cm}^2 \cdot \text{g}^{-1}$ , respectively. Compared to some

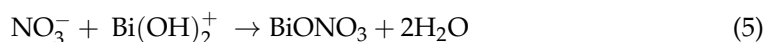
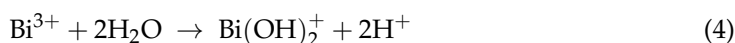
recent methods in the literature, the sonochemically fabricated BiOI showed better surface properties [27,37–39]. One of the main goals of using BiOI as a photocatalyst is to displace the harmful ultraviolet light with the safe-visible light. Due to that, the optical properties of BiOI were studied in the range of 300 nm to 800 nm. The Tauc plot (Equation (2)) was employed in determining the bandgap-energy ( $E_g$ ) for the synthesized photocatalyst. As monitored in Figure 4d, the  $E_g$  was 1.835 eV, which is within the typical  $E_g$  range for BiOI [40–43]. These results nominated the prepared BiOI nanoparticles as a possible photocatalyst within the visible light region.

$$\alpha h\gamma = A(h\gamma - E_g)^{n/2} \quad (2)$$

where:  $h$  represents the Plank constant,  $\alpha$  and  $\gamma$  are the absorption coefficient and photonic frequency;  $n$  is an interband transition constant (for BiOI,  $n = 1$ ) [44].

### 3.2. Possible Formation Route of BiOI Nanoparticles

Preparing a nanoscale BiOI is one of the essential targets to enhance photocatalytic performance. The long digestion time in the mother solution may produce larger particles; therefore, short digestion times are crucial for obtaining nanosized particles. This method prepared BiOI nanoparticles by avoiding heating and long digestion time; in addition to that, sonication was employed to prevent the formation of large particles and disintegrate the formed ones. In addition, triethylene glycol was used to obtain a clear solution and may serve as a surfactant for additional prevention of particle lumping. The formation route for BiOI can be explained by Equations (3)–(6) [26].



### 3.3. Adsorption of IC on the BiOI

The effect of contact time on IC sorption by the prepared BiOI is depicted in Figure 5a. The adsorption trend increased progressively until 60 min, which was almost sufficient to reach equilibrium. Figure 5b showed that the obtained  $q_t$  value increased proportionally with the IC concentration until it reached  $184.95 \text{ mg}\cdot\text{g}^{-1}$  with the  $100 \text{ mg L}^{-1}$ . This high  $q_t$  with the more concentrated dye solution indicated the usability of this nanomaterial for the removal of dyes from industrial wastewater where high pollutant concentrations were expected.

The influence of temperature on IC sorption by BiOI was investigated (Figure 5b). The inverse proportionality of  $q_t$  with the temperature of the solution implies the exothermic nature of sorption [45].

Figure 5c illustrates the impact of solution pH on the sorption process. The obtained  $q_t$  values indicated the suitability of pH 6 for the IC adsorption on the sonochemically-synthesized BiOI. With the low pH values (high  $\text{H}^+$  concentration), the electron-rich sites on the dye and/or BiOI may be protonated. On the other hand, at high pH values (high  $\text{OH}^-$  concentration), the hydroxyl groups may compete with pollutants on the adsorption sites of sorbent.

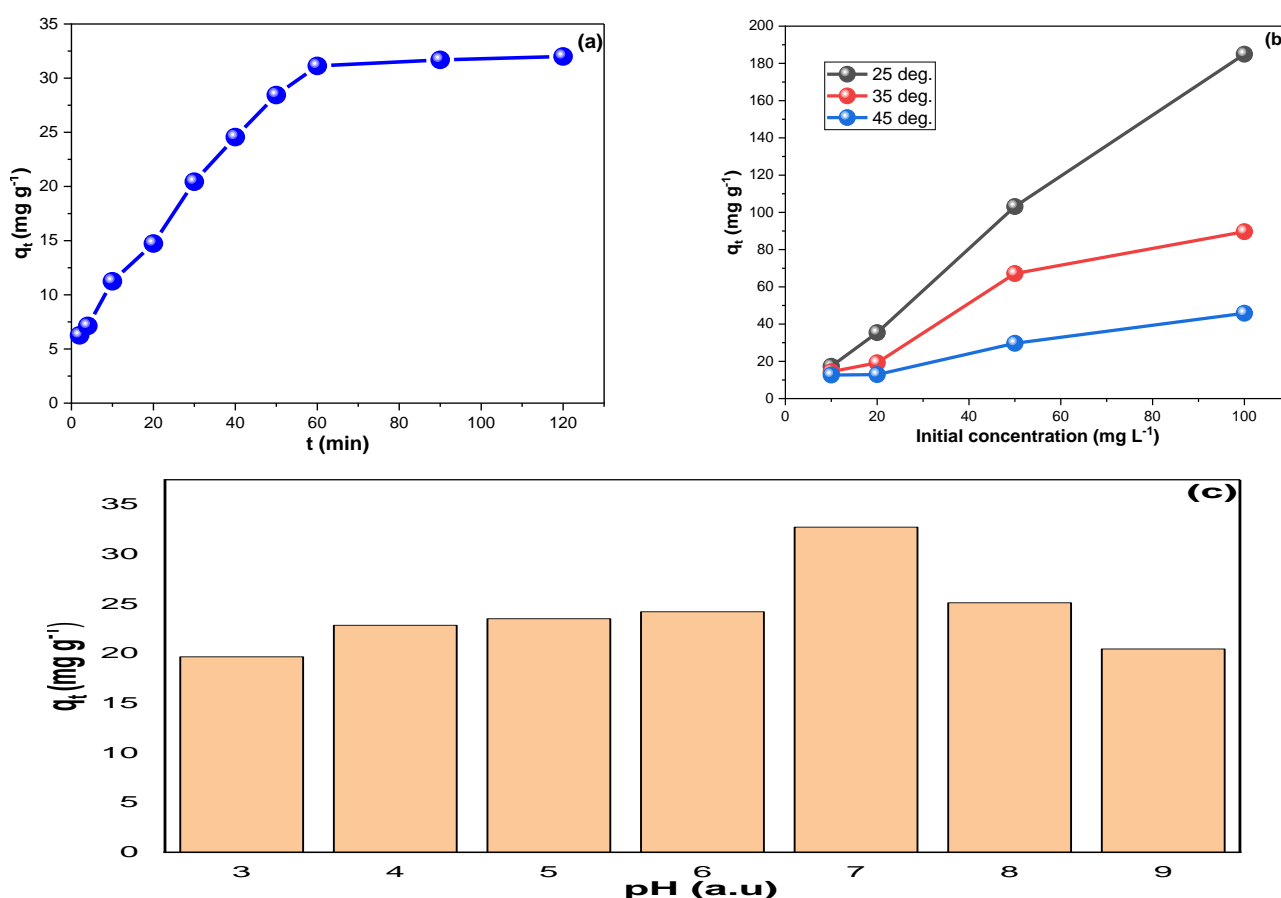


**Figure 5.** The influence of (a) contact time, (b) concentration at different temperatures, and (c) pH on the adsorption of IC on BiOI nanoparticles.

### 3.4. Adsorption Kinetics

The adsorption capacity, which is the milligrams of pollutant adsorbed per one gram of sorbent (*q<sub>t</sub>*, in mg·g<sup>-1</sup>), was calculated via Equation (7). The pseudo-first-order (PSFO) and pseudo-second-order (PSSO) kinetic models (Equations (8) and (9)) were used to explore the adsorption rate. An examination of the rate-control mechanism for adsorption was carried out via the liquid-film-diffusion model (LFD) (Equation (10)) and the intraparticle-diffusion model (IPD) (Equation (11)) [46,47].

$$q_t = \frac{(C_0 - C_t) V}{m} \quad (7)$$

$$\ln(q_e - q_t) = \ln q_e - k_1 \cdot t \quad (8)$$

$$\frac{1}{q_t} = \frac{1}{k_2 \cdot q_e^2 \cdot t} + \frac{1}{q_e} \quad (9)$$

$$q_t = K_{IP} \times t^{1/2} + C_i \quad (10)$$

$$\ln(1 - F) = -K_{LF} \times t \quad (11)$$

where: *m*, *v*, *C<sub>t</sub>*, and *C<sub>0</sub>* were sorbent mass (g), solution volume (mL), and solution concentration (mg L<sup>-1</sup>) at time *t* and zero, respectively; *q<sub>e</sub>* (mg·g<sup>-1</sup>) represent the adsorption capacity at equilibrium; *k<sub>1</sub>* (min<sup>-1</sup>), *k<sub>2</sub>* (g mg<sup>-1</sup> min<sup>-1</sup>), *k<sub>ip</sub>* (mg·g<sup>-1</sup> min<sup>-1/2</sup>), and *k<sub>LF</sub>* (min<sup>-1</sup>) are the PSFO, PSSO, IPDM, and the LFD constants, respectively. *C<sub>i</sub>* (mg·g<sup>-1</sup>) is the boundary layer factor.

Figure 6a,b illustrated the linear plot for the PSFO and PSSO kinetic models. The *R*<sup>2</sup> values were 0.948 and 0.873 for the PSFO and PSSO, while their *q<sub>t</sub>* values were

46.282 mg g<sup>-1</sup> and 4.348 mg·g<sup>-1</sup>, respectively. These findings showed that the IC adsorption on BiOI obeyed the PSFO kinetic model [48]. The investigation of the step control mechanism of IC adsorption on BiOI was monitored in Figure 6c,d, and the Supplementary (Table S1). The IPDM and LFDM exhibited equilibrium constants of 4.367 mg·g<sup>-1</sup> min<sup>-1/2</sup> and 0.053 min<sup>-1</sup>, respectively. The R<sup>2</sup> values were 0.965 and 0.948 for IPDM and LFDM, suggesting that IPDM controlled the IC sorption. These results indicated that IC adsorption mainly depends on the migration from the solution to the sorbent's surface, supporting the PSFO agreement. Nevertheless, the obtained C<sub>i</sub> value of 0.533 indicated slight participation of LFDM in controlling the IC sorption on BiOI [49].

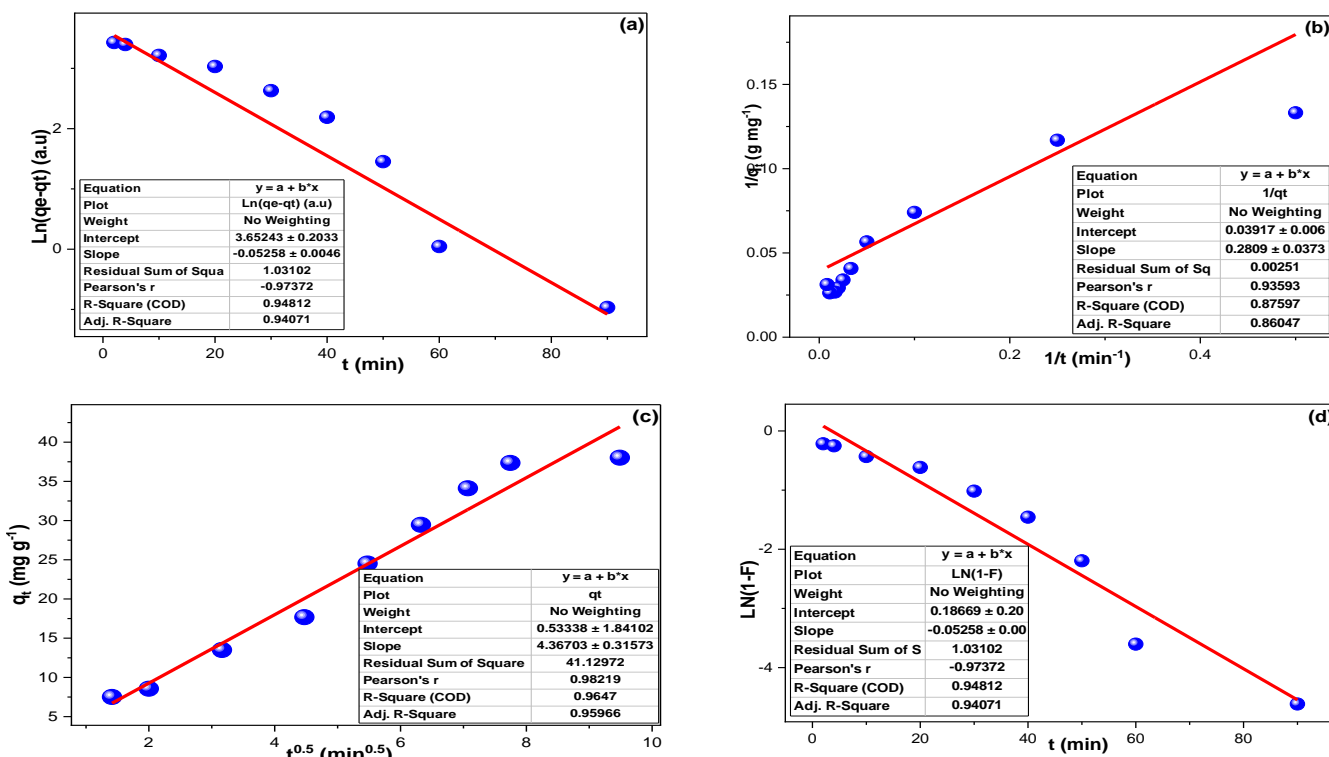


**Figure 6.** (a) PSFO, (b) PSSO, (c) IPDM, and (d) LFDM investigations for the adsorption of IC on BiOI nanoparticles.

### 3.5. Adsorption Isotherms

Many models have been used in describing the adsorption isotherms. Among these, the Langmuir (LIM, Equation (12)) and Freundlich (FIM, Equation (13)) are frequently used, which is the case in this study.

$$\frac{1}{q_e} = \frac{1}{K_L q_m} \cdot \frac{1}{C_e} + \frac{1}{K_L} \quad (12)$$

$$\ln q_e = \ln K_F + \frac{1}{n} \ln C_e \quad (13)$$

K<sub>L</sub> (L mg<sup>-1</sup>) and K<sub>F</sub> (L mg<sup>-1</sup>) represented the LIM and FIM constants. C<sub>e</sub> (mg L<sup>-1</sup>) is the pollutant's concentration at equilibrium, q<sub>m</sub> (mg·g<sup>-1</sup>) is the maximum adsorption capacity, while n (arbitrary) is the Freundlich-heterogeneity factor.

Figure 7 showed the plots of LIM and FIM, and their calculated parameters were included in (Table S1). The adsorption of IC on BiOI fitted the LIM with an R<sup>2</sup> of 0.943. On the contrary, the FIM findings of R<sup>2</sup> and (1/n) values of 0.878 and 1.125 indicate that the multilayer sorption was unfavorable [50–54].

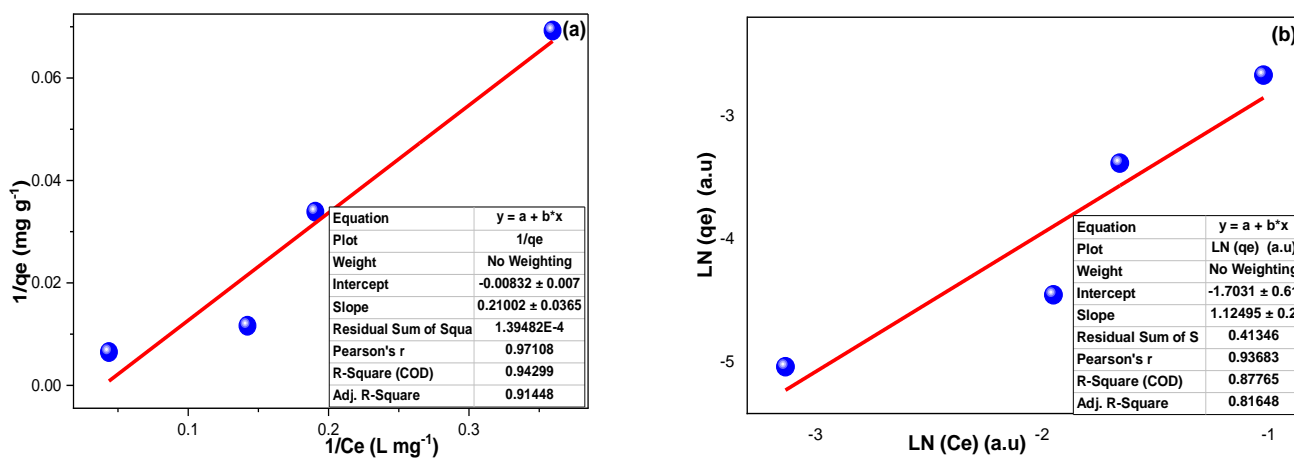


**Figure 7.** (a) Langmuir isotherm and (b) the Freundlich isotherm for IC adsorption on BiOI at 25 °C using 10, 20, 50, and 100 mg L<sup>-1</sup> IC solutions.

### 3.6. Thermodynamic

The thermodynamics was explored to better understand the adsorption of IC onto the fabricated BiOI (Figure 8). Equation (14) was employed to compute the entropy ( $\Delta S^\circ$ ) and enthalpy ( $\Delta H^\circ$ ), then after the Gibbs free energy ( $\Delta G^\circ$ ) was calculated by applying their values in Equation (15), and the obtaining were gathered in (Table S1).

$$\ln K_c = \frac{\Delta H^\circ}{RT} + \frac{\Delta S^\circ}{R} \quad (14)$$

$$\Delta G^\circ = \Delta H^\circ - T \Delta S^\circ \quad (15)$$

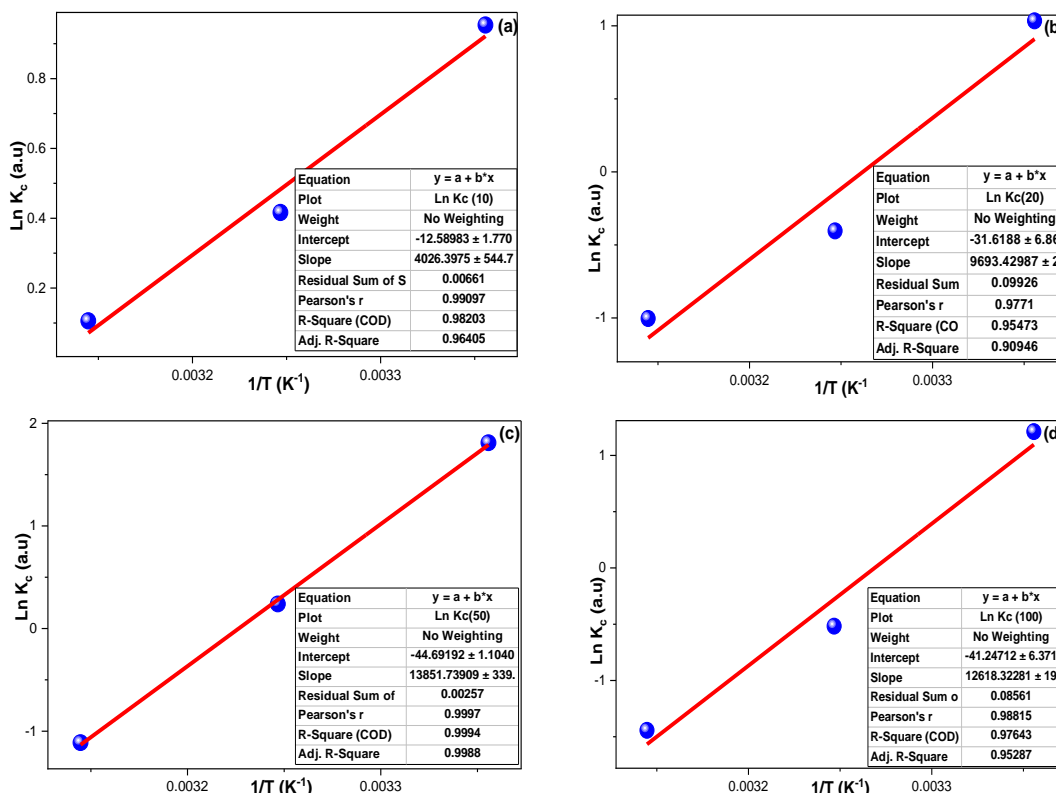


**Figure 8.** The thermodynamic investigation for IC adsorption on BiOI at 25 °C, 35 °C, and 45 °C for (a) 10, (b) 20, (c) 50, and (d) 100 mg L<sup>-1</sup> solutions.

The value of ideal-gas-constant R was applied as  $0.0081345 \text{ kJ mol}^{-1}$  in all calculations. The computed  $\Delta H^\circ$  values for 10, 25, 50, and  $100 \text{ mg L}^{-1}$  were  $-33.477$ ,  $-80.596$ ,  $-115.170$ , and  $104.915 \text{ kJ mol}^{-1}$ , respectively, indicating exothermic sorption. In addition, the  $\Delta G^\circ$  values for these concentrations were  $-2.283$ ,  $-2.253$ ,  $-4.436$ , and  $-2.736 \text{ kJ mol}^{-1}$ , indicating the spontaneity of adsorptions at low temperature, and supporting the exothermic finding [55–59]. The decrease of  $\Delta G^\circ$  proportionally with the concentration encourages using this sorbent for water treatment. Furthermore, the chemisorption nature of this process can be predicted from the  $\Delta H^\circ$  values of more than  $80 \text{ kJ mol}^{-1}$ .

### 3.7. Photocatalytic Degradation of IC under Visible Light

According to some recent studies, the generation of reactive hydroxyl radicals requires about 1.9 electron volt that BiOI nanoparticles can provide, according to the obtained  $E_g$  [60–62]. In order to assess the kinetic order of the photoreaction, a UV-vis spectrophotometer was used to monitor the IC concentration. Figure 9a illustrated the first-order kinetic study expressed by Equation (16).

$$\ln \frac{C_t}{C_0} = kt \quad (16)$$

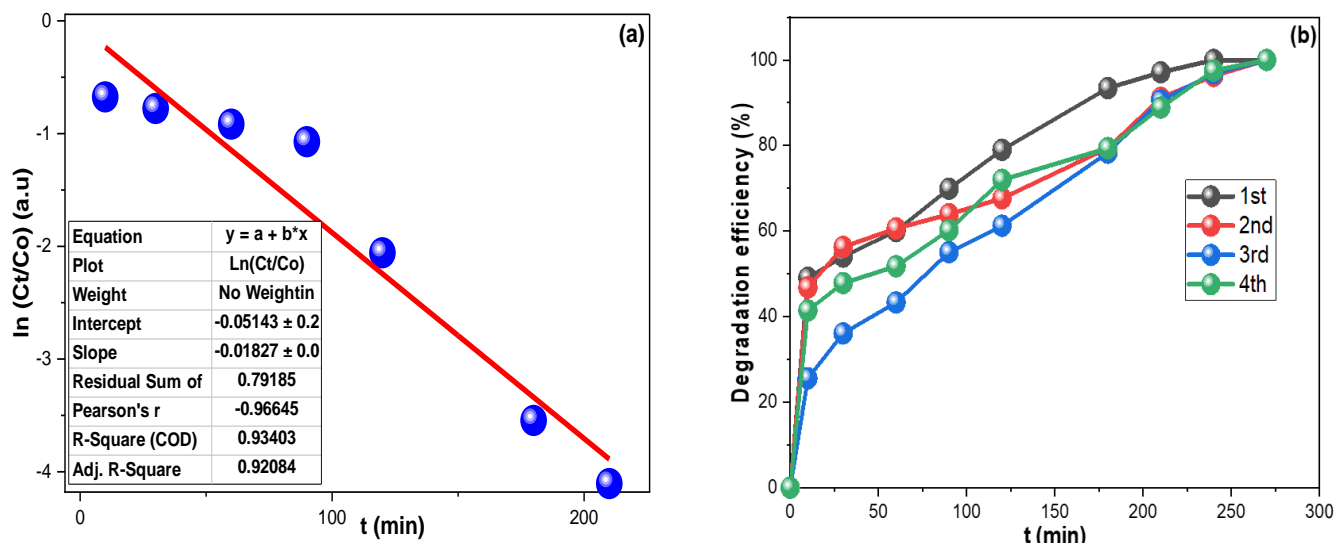


**Figure 9.** (a) The first-order kinetic investigation and (b) reuse study for BiOI in degrading IC in water under artificial visible light.

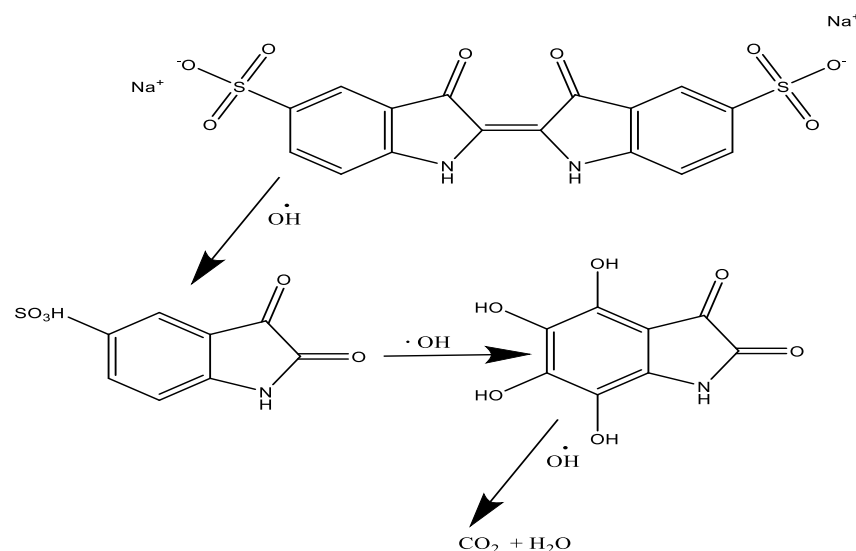
$C_0$  and  $C_t$  represent the IC concentrations at time zero and  $t$  (min), while  $k_1$  is the first-order rate constant. The photocatalytic elimination of IC in water fitted the first-order model with a good agreement ( $R^2 = 0.934$ , and a  $k_1 = 1.83 \times 10^{-2} \text{ min}^{-1}$ ). 93% of the IC was degraded efficiently within three hours, while the complete elimination of the IC was accomplished within four hours. Compared to previous literature findings, the sonochemical-BiOI possessed competitive results (Table 1). Furthermore, the BiOI photocatalyst was tested for reuse in degrading IC in four consecutive batches of spiked water (Figure 9b). The used BiOI was filtered, washed with 100 mL of distilled water, and reused again. Compared to the virgin batch, only a 30 min delay was found within the reuse durations. These results demonstrated that the sonochemical-BiOI is highly effective for degrading IC in polluted water. Possibly, some degradation products suppressed part of the active photocatalyst sites, resulting in this typical slight reduction [63,64].

**Table 1.** Compares the photocatalysts' photodegradation with the sonochemically fabricated BiOI in this study.

Nanomaterial	Pollutant	Photodegradation Percentage/Time	Reference
BiOI	Indigo carmine	93% within 180 min	This study
BiOI	Rhodamine B	81% within 180 min	[65]
BiOI	Methyl orange	40% within 180 min	[44]
BiOI	Phenol	87% in 180 min	[21]
BiOI	Tetracycline	33% within 120 min	[63]
CuFe <sub>2</sub> O <sub>4</sub>	Indigo carmine	35% within 120 min	[66]
CuFe <sub>2</sub> O <sub>4</sub> -1% Zr	Indigo carmine	46% within 120 min	[66]
CuFe <sub>2</sub> O <sub>4</sub> -3% Zr	Indigo carmine	55% within 120 min	[66]
CuFe <sub>2</sub> O <sub>4</sub> -5% Zr	Indigo carmine	71% within 120 min	[66]

### 3.8. Mechanism of Photocatalytic Degradation

The TOC was used to investigate the photocatalytic degradation of IC, and the Perkin Elmer 2400 CHNS organic elemental analyzer (USA) was employed for this purpose. The standard 50 mg L<sup>-1</sup> results for carbon and nitrogen were 0.12% and 0.02%, respectively. Following degradation, an aliquot was filtered, while a second aliquot containing the BiOI suspension was analyzed to determine the fate of the adsorbed IC. After degradation, both samples showed a 0.0% carbon and nitrogen content. These findings indicated that The IC had been mineralized to CO<sub>2</sub> and H<sub>2</sub>O. Based on the TOC findings, the visible light irradiation may generate holes (h<sup>+</sup>) and electrons (e<sup>-</sup>) in the valence and conduction bands (VBs and CBs) of the BiOI nanoparticles. The h<sup>+</sup> may interact with H<sub>2</sub>O/OH<sup>-</sup> and produced hydroxyl radicals (OH<sup>•</sup>) known for their capability to degrade IC in water [67,68]. The following Scheme 1 illustrates a possible route for the mineralization of IC.



**Scheme 1.** The proposed degradation route for IC dye under visible light using the prepared BiOI nanoparticles.

## 4. Conclusions

An energy-saving and fast sonochemical method was successfully used to prepare BiOI nanoparticles entirely at room temperature. This method eliminated the time- and energy-consuming incubation step in mutual preparation practices. The resulting BiOI was about 20 nm in diameter, with a surface area of 34.03 m<sup>2</sup> g<sup>-1</sup> and an energy gap of 1.887 eV. The adsorption of IC on BiOI fitted the PSFO, and the intraparticle diffusion step controlled the adsorption. Moreover, the BiOI showed an adsorption capacity of 185 mg g<sup>-1</sup>. The thermodynamic data indicated that the sorption was spontaneous and exothermic. In

addition, the BiOI showed an excellent photocatalytic activity by degrading 93% of the IC within 180 min under visible light. The consistent high efficiency indicated the feasibility of using BiOI within the four reuse cycles. The TOC results revealed that IC was completely mineralized under artificial visible light using the Sonochemically prepared BiOI.

**Supplementary Materials:** The following supporting information can be downloaded at: <https://www.mdpi.com/article/10.3390/inorganics10050065/s1>, Table S1: The obtained parameters for the adsorption kinetics, isotherms, and thermodynamics of the IC sorption on the BiOI nanoparticles.

**Author Contributions:** Conceptualization, M.R.E. and B.Y.A.; methodology, N.Y.E., F.A.A. and A.H.A.; software, B.Y.A.; investigation, K.H.I., N.Y.E. and F.A.A.; writing—original draft preparation, review and editing, M.R.E. and B.Y.A.; supervision, and funding acquisition, M.R.E. All authors have read and agreed to the published version of the manuscript.

**Funding:** This research was supported by the Deanship of Scientific Research, Imam Mohammad Ibn Saud Islamic University, Saudi Arabia, Grant No RG-21-09-74.

**Data Availability Statement:** The data of this article is available from the corresponding author under reasonable request.

**Conflicts of Interest:** The authors declare that they have no known competing financial interest or personal relationship.

## References

- Makowskaa, M.; Sowinskab, A. Characteristics of organic pollutants in wastewater from individual treatment systems. *Methods* **2020**, *8*, 12. [[CrossRef](#)]
- Khader, E.H.; Mohammed, T.J.; Mirghaffari, N.; Salman, A.D.; Juzsakova, T.; Abdullah, T.A. Removal of organic pollutants from produced water by batch adsorption treatment. *Clean Technol. Environ. Policy* **2022**, *24*, 713–720. [[CrossRef](#)]
- Goździejewska, A.M.; Gwoździk, M.; Kulesza, S.; Bramowicz, M.; Koszalka, J. Effects of suspended micro-and nanoscale particles on zooplankton functional diversity of drainage system reservoirs at an open-pit mine. *Sci. Rep.* **2019**, *9*, 1–13. [[CrossRef](#)] [[PubMed](#)]
- Ho, S. Removal of Dyes from Wastewater by Adsorption onto Activated Carbon: Mini Review. *J. Geosci. Environ. Prot.* **2020**, *8*, 120. [[CrossRef](#)]
- Saleh, I.A.; Zouari, N.; Al-Ghouti, M. Removal of pesticides from water and wastewater: Chemical, physical and biological treatment approaches. *Environ. Technol. Innov.* **2020**, *19*, 101026. [[CrossRef](#)]
- Abuhasel, K.; Kchaou, M.; Alquraish, M.; Munusamy, Y.; Jeng, Y.T. Oily wastewater treatment: Overview of conventional and modern methods, challenges, and future opportunities. *Water* **2021**, *13*, 980. [[CrossRef](#)]
- Zango, Z.U.; Jumbri, K.; Sambudi, N.S.; Ramli, A.; Abu Bakar, N.H.H.; Saad, B.; Rozaini, M.N.H.; Isiyaka, H.A.; Jagaba, A.H.; Aldaghri, O. A critical review on metal-organic frameworks and their composites as advanced materials for adsorption and photocatalytic degradation of emerging organic pollutants from wastewater. *Polymers* **2020**, *12*, 2648. [[CrossRef](#)]
- Mansouri, F.; Chouchene, K.; Roche, N.; Ksibi, M. Removal of Pharmaceuticals from Water by Adsorption and Advanced Oxidation Processes: State of the Art and Trends. *Appl. Sci.* **2021**, *11*, 6659. [[CrossRef](#)]
- Naseem, T.; Durrani, T. The role of some important metal oxide nanoparticles for wastewater and antibacterial applications: A review. *Environ. Chem. Ecotoxicol.* **2021**, *3*, 59–75. [[CrossRef](#)]
- Palani, G.; Arputhalatha, A.; Kannan, K.; Lakkaboyana, S.K.; Hanafiah, M.M.; Kumar, V.; Marella, R. Current trends in the application of nanomaterials for the removal of pollutants from industrial wastewater treatment—A review. *Molecules* **2021**, *26*, 2799. [[CrossRef](#)]
- Li, K.; Liu, Q.; Cheng, H.; Hu, M.; Zhang, S. Classification and carbon structural transformation from anthracite to natural coaly graphite by XRD, Raman spectroscopy, and HRTEM. *Spectrochim. Acta Part A Mol. Biomol. Spectrosc.* **2021**, *249*, 119286. [[CrossRef](#)] [[PubMed](#)]
- Yao, L.; Yang, H.; Chen, Z.; Qiu, M.; Hu, B.; Wang, X. Bismuth oxychloride-based materials for the removal of organic pollutants in wastewater. *Chemosphere* **2021**, *273*, 128576. [[CrossRef](#)] [[PubMed](#)]
- Arumugam, M.; Choi, M.Y. Recent progress on bismuth oxyiodide (BiOI) photocatalyst for environmental remediation. *J. Ind. Eng. Chem.* **2020**, *81*, 237–268. [[CrossRef](#)]
- Narenuch, T.; Senasu, T.; Chankhaniththa, T.; Nanai, S. Sunlight-Active BiOI Photocatalyst as an Efficient Adsorbent for the Removal of Organic Dyes and Antibiotics from Aqueous Solutions. *Molecules* **2021**, *26*, 5624. [[CrossRef](#)]
- Lv, Y.; Li, P.; Che, Y.; Hu, C.; Ran, S.; Shi, P.; Zhang, W. Facile Preparation and Characterization of Nanostructured BiOI microspheres with certain adsorption-photocatalytic properties. *Mater. Res.* **2018**, *21*, 1–9. [[CrossRef](#)]
- Wang, X.; Zhou, C.; Yin, L.; Zhang, R.; Liu, G. Iodine-deficient BiOI nanosheets with lowered valence band maximum to enable visible light photocatalytic activity. *ACS Sustain. Chem. Eng.* **2019**, *7*, 7900–7907. [[CrossRef](#)]

17. Hu, J.; Weng, S.; Zheng, Z.; Pei, Z.; Huang, M.; Liu, P. Solvents mediated-synthesis of BiOI photocatalysts with tunable morphologies and their visible-light driven photocatalytic performances in removing of arsenic from water. *J. Hazard. Mater.* **2014**, *264*, 293–302. [[CrossRef](#)]
18. Algethami, F.K.; Elamin, M.R.; Abdulkhair, B.Y.; Al-Zharani, M.; Qarah, N.A.; Alghamdi, M.A. Fast fabrication of bismuth oxyiodide/carbon-nanofibers composites for efficient anti-proliferation of liver and breast cancer cells. *Z. Für Anorg. Und Allg. Chem.* **2021**, *647*, 1921–1929. [[CrossRef](#)]
19. Di, J.; Xia, J.; Ge, Y.; Xu, L.; Xu, H.; He, M.; Zhang, Q.; Li, H. Reactable ionic liquid-assisted rapid synthesis of BiOI hollow microspheres at room temperature with enhanced photocatalytic activity. *J. Mater. Chem. A* **2014**, *2*, 15864–15874. [[CrossRef](#)]
20. Long, Y.; Wang, Y.; Zhang, D.; Ju, P.; Sun, Y. Facile synthesis of BiOI in hierarchical nanostructure preparation and its photocatalytic application to organic dye removal and biocidal effect of bacteria. *J. Colloid Interface Sci.* **2016**, *481*, 47–56. [[CrossRef](#)]
21. Wang, X.; Zhang, Y.; Zhou, C.; Huo, D.; Zhang, R.; Wang, L. Hydroxyl-regulated BiOI nanosheets with a highly positive valence band maximum for improved visible-light photocatalytic performance. *Appl. Catal. B Environ.* **2020**, *268*, 118390. [[CrossRef](#)]
22. Lee, W.W.; Lu, C.-S.; Chuang, C.-W.; Chen, Y.-J.; Fu, J.-Y.; Siao, C.-W.; Chen, C.-C. Synthesis of bismuth oxyiodides and their composites: Characterization, photocatalytic activity, and degradation mechanisms. *RSC Adv.* **2015**, *5*, 23450–23463. [[CrossRef](#)]
23. Deng, Z.; Chen, D.; Peng, B.; Tang, F. From bulk metal Bi to two-dimensional well-crystallized BiOX (X = Cl, Br) micro-and nanostructures: Synthesis and characterization. *Cryst. Growth Des.* **2008**, *8*, 2995–3003. [[CrossRef](#)]
24. Chou, S.-Y.; Chen, C.-C.; Dai, Y.-M.; Lin, J.-H.; Lee, W.W. Novel synthesis of bismuth oxyiodide/graphitic carbon nitride nanocomposites with enhanced visible-light photocatalytic activity. *RSC Adv.* **2016**, *6*, 33478–33491. [[CrossRef](#)]
25. Chen, C.-C.; Fu, J.-Y.; Chang, J.-L.; Huang, S.-T.; Yeh, T.-W.; Hung, J.-T.; Huang, P.-H.; Liu, F.-Y.; Chen, L.-W. Bismuth oxyfluoride/bismuth oxyiodide nanocomposites enhance visible-light-driven photocatalytic activity. *J. Colloid Interface Sci.* **2018**, *532*, 375–386. [[CrossRef](#)]
26. Sun, X.; Wu, J.; Liu, Q.; Tian, F. Mechanism insights into the enhanced activity and stability of hierarchical bismuth oxyiodide microspheres with selectively exposed (0 0 1) or (1 1 0) facets for photocatalytic oxidation of gaseous mercury. *Appl. Surf. Sci.* **2018**, *455*, 864–875. [[CrossRef](#)]
27. Xiao, Y.; Wu, J.; Jia, T.; Li, T.; Wang, Z.; Qi, Y.; Liu, Q.; Qi, X.; He, P. Fabrication of BiOI nanosheets with exposed (001) and (110) facets with different methods for photocatalytic oxidation elemental mercury. *Colloids Interface Sci. Commun.* **2021**, *40*, 100357. [[CrossRef](#)]
28. Gao, F.; Zeng, D.; Huang, Q.; Tian, S.; Xie, C. Chemically bonded graphene/BiOCl nanocomposites as high-performance photocatalysts. *Phys. Chem. Chem. Phys.* **2012**, *14*, 10572–10578. [[CrossRef](#)]
29. Song, J.-M.; Mao, C.-J.; Niu, H.-L.; Shen, Y.-H.; Zhang, S.-Y. Hierarchical structured bismuth oxychlorides: Self-assembly from nanoplates to nanoflowers via a solvothermal route and their photocatalytic properties. *CrystEngComm* **2010**, *12*, 3875–3881. [[CrossRef](#)]
30. Sun, S.; Liang, F.; Tang, L.; Wu, J.; Ma, C. Microstructural investigation of gas shale in Longmaxi formation, Lower Silurian, NE Sichuan basin, China. *Energy Explor. Exploit.* **2017**, *35*, 406–429. [[CrossRef](#)]
31. Thommes, M.; Kaneko, K.; Neimark, A.V.; Olivier, J.P.; Rodriguez-Reinoso, F.; Rouquerol, J.; Sing, K.S.W. Physisorption of gases, with special reference to the evaluation of surface area and pore size distribution (IUPAC Technical Report). *Pure Appl. Chem.* **2015**, *87*, 1051–1069. [[CrossRef](#)]
32. Yang, Z.; Zhang, J.; Zhang, X.; Wang, L.; Chao, L. Preparation and Properties of BiOI with High Sorption Capacity. *J. Wuhan Univ. Technol. Sci. Ed.* **2020**, *35*, 620–628. [[CrossRef](#)]
33. Yang, J.; Su, H.; Wu, Y.; Li, D.; Zhang, D.; Sun, H.; Yin, S. Facile Synthesis of Kermesinus BiOI with Oxygen Vacancy for Efficient Hydrogen Generation. *Chem. Eng. J.* **2020**, *420*, 127607. [[CrossRef](#)]
34. Wang, X.; Guo, Z.; Zhang, C.; Zhu, S.; Li, L.; Gu, Z.; Zhao, Y. Ultrasmall BiOI quantum dots with efficient renal clearance for enhanced radiotherapy of cancer. *Adv. Sci.* **2020**, *7*, 1902561. [[CrossRef](#)] [[PubMed](#)]
35. Zhang, H.; Yang, J.; Guo, L.; Wang, R.; Peng, S.; Wang, J.; Wan, J.; Xu, J. Microwave-Aided Synthesis of BiOI/g-C3N4 Composites and Their Enhanced Catalytic Activities for Cr (VI) Removal. *Chem. Phys. Lett.* **2020**, *762*, 138143. [[CrossRef](#)]
36. Bargozideh, S.; Tasviri, M.; Ghahraei, M. Effect of carbon nanotubes loading on the photocatalytic activity of BiSI/BiOI as a novel photocatalyst. *Environ. Sci. Pollut. Res.* **2020**, *27*, 36754–36764. [[CrossRef](#)]
37. Liu, J.; Huang, L.; Li, Y.; Yang, L.; Wang, C.; Liu, J.; Song, Y.; Tian, Q.; Li, H. Fabrication oxygen defect-mediated double Z-scheme BiOI/BiO<sub>2-x</sub>/BiOBr photocatalyst for pollutions degradation and bacteria inactivation. *J. Environ. Chem. Eng.* **2021**, *10*, 106668. [[CrossRef](#)]
38. Amiri, O.; Beshkar, F.; Ahmed, S.S.; Mahmood, P.H.; Dezaye, A.A. Hierarchical p-BiOI/n-BiPO<sub>4</sub> heterojunction nanocomposite with enhanced visible-light photocatalytic desulfurization of thiophene under mild conditions. *Int. J. Hydrg. Energy* **2021**, *46*, 6547–6560. [[CrossRef](#)]
39. Guan, Y.; Wu, J.; Man, X.; Liu, Q.; Qi, Y.; He, P.; Qi, X. Rational fabrication of flower-like BiOI<sub>1-x</sub> photocatalyst by modulating efficient iodine vacancies for mercury removal and DFT study. *Chem. Eng. J.* **2020**, *396*, 125234. [[CrossRef](#)]
40. Mehrali-Afjani, M.; Nezamzadeh-Ejhieh, A.; Aghaei, H. A brief study on the kinetic aspect of the photodegradation and mineralization of BiOI-Ag<sub>3</sub>PO<sub>4</sub> towards sodium diclofenac. *Chem. Phys. Lett.* **2020**, *759*, 137873. [[CrossRef](#)]
41. Jeevanantham, N.; Balasundaram, O.N. High-performance visible light photocatalytic activity of cobalt (Co) doped CdS nanoparticles by wet chemical route. *J. Iran. Chem. Soc.* **2019**, *16*, 243–251. [[CrossRef](#)]

42. Sabonian, M.; Mahanpoor, K. Preparation of ZnO nanocatalyst supported on todorokite and photocatalytic efficiency in the reduction of chromium (VI) pollutant from aqueous solution. *Iran. J. Catal.* **2019**, *9*, 201–211.
43. Zeng, L.; Zhe, F.; Wang, Y.; Zhang, Q.; Zhao, X.; Hu, X.; Wu, Y.; He, Y. Preparation of interstitial carbon doped BiOI for enhanced performance in photocatalytic nitrogen fixation and methyl orange degradation. *J. Colloid Interface Sci.* **2019**, *539*, 563–574. [CrossRef] [PubMed]
44. Cheng, H.; Huang, B.; Dai, Y.; Qin, X.; Zhang, X. One-step synthesis of the nanostructured AgI/BiOI composites with highly enhanced visible-light photocatalytic performances. *Langmuir* **2010**, *26*, 6618–6624. [CrossRef]
45. Darryle, C.M.; Acyanka, E.; Takam, B.; Line, L.N.; Kamgang, G.Y.; Laminsi, S.; Sellaoui, L.; Bonilla-Petriciolet, A. Influence of plasma-based surface functionalization of palm fibers on the adsorption of diclofenac from water: Experiments, thermodynamics and removal mechanism. *J. Water Process Eng.* **2021**, *43*, 102254. [CrossRef]
46. Elamin, M.R.; Abdulkhair, B.Y.; Elzupir, A.O. Insight to aspirin sorption behavior on carbon nanotubes from aqueous solution: Thermodynamics, kinetics, influence of functionalization and solution parameters. *Sci. Rep.* **2019**, *9*, 1–10. [CrossRef] [PubMed]
47. Acharya, J.; Sahu, J.; Mohanty, C.; Meikap, B. Removal of lead (II) from wastewater by activated carbon developed from Tamarind wood by zinc chloride activation. *Chem. Eng. J.* **2009**, *149*, 249–262. [CrossRef]
48. Kyzas, G.Z.; Deliyanni, E.A. Modified activated carbons from potato peels as green environmental-friendly adsorbents for the treatment of pharmaceutical effluents. *Chem. Eng. Res. Des.* **2015**, *97*, 135–144. [CrossRef]
49. An, B.J.P. Cu (II) and As (V) adsorption kinetic characteristic of the multifunctional amino groups in chitosan. *Processes* **2020**, *8*, 1194. [CrossRef]
50. Hamdaoui, O.; Naffrechoux, E. Modeling of adsorption isotherms of phenol and chlorophenols onto granular activated carbon: Part I. Two-parameter models and equations allowing determination of thermodynamic parameters. *J. Hazard. Mater.* **2007**, *147*, 381–394. [CrossRef]
51. Kumar, P.S.; Ramalingam, S.; Senthamarai, C.; Niranjanaa, M.; Vijayalakshmi, P.; Sivanesan, S. Adsorption of dye from aqueous solution by cashew nut shell: Studies on equilibrium isotherm, kinetics and thermodynamics of interactions. *Desalination* **2010**, *261*, 52–60. [CrossRef]
52. Aljeboree, A.M.; Alshirifi, A.N.; Alkaim, A.F. Kinetics and equilibrium study for the adsorption of textile dyes on coconut shell activated carbon. *Arab. J. Chem.* **2017**, *10*, S3381–S3393. [CrossRef]
53. Jain, S.N.; Shaikh, Z.; Mane, V.S.; Vishnoi, S.; Mawal, V.N.; Patel, O.R.; Bhandari, P.S.; Gaikwad, M. Nonlinear regression approach for acid dye remediation using activated adsorbent: Kinetic, isotherm, thermodynamic and reusability studies. *Microchem. J.* **2019**, *148*, 605–615. [CrossRef]
54. Do, D.D. *Adsorption Analysis: Equilibria and Kinetics*; Imperial College Press: London, UK, 1998; Volume 2.
55. Letshwenyo, M.W.; Mokgosi, S. Investigation of water treatment sludge from drinking water treated with Zetafloc 553I coagulant for phosphorus removal from wastewater. *J. Environ. Manag.* **2021**, *282*, 111909. [CrossRef] [PubMed]
56. Demirbas, O.; Calimli, M.H.; Kuyuldar, E.; Alma, M.H.; Nas, M.S.; Sen, F. Equilibrium, kinetics, and thermodynamic of adsorption of enzymes on diatomite clay materials. *BioNanoScience* **2019**, *9*, 474–482. [CrossRef]
57. Aarab, N.; Hsini, A.; Essekri, A.; Laabd, M.; Lakhmiri, R.; Albourine, A. Removal of an emerging pharmaceutical pollutant (metronidazole) using PPY-PANI copolymer: Kinetics, equilibrium and DFT identification of adsorption mechanism. *Groundw. Sustain. Dev.* **2020**, *11*, 100416. [CrossRef]
58. Vasudevan, S.; Lakshmi, J. Studies relating to an electrochemically assisted coagulation for the removal of chromium from water using zinc anode. *Water Supply* **2011**, *11*, 142–150. [CrossRef]
59. Inglezakis, V.J.; Zorpas, A.A. Heat of adsorption, adsorption energy and activation energy in adsorption and ion exchange systems. *Desalination Water Treat.* **2012**, *39*, 149–157. [CrossRef]
60. Wen, J.; Xie, J.; Chen, X.; Li, X. A review on g-C<sub>3</sub>N<sub>4</sub>-based photocatalysts. *Appl. Surf. Sci.* **2017**, *391*, 72–123. [CrossRef]
61. Wang, C.; Zhang, X.; Liu, Y. Promotion of multi-electron transfer for enhanced photocatalysis: A review focused on oxygen reduction reaction. *Appl. Surf. Sci.* **2015**, *358*, 28–45. [CrossRef]
62. Jiang, D.; Chen, L.; Zhu, J.; Chen, M.; Shi, W.; Xie, J. Novel p-n heterojunction photocatalyst constructed by porous graphite-like C<sub>3</sub>N<sub>4</sub> and nanostructured BiOI: Facile synthesis and enhanced photocatalytic activity. *Dalton Trans.* **2013**, *42*, 15726–15734. [CrossRef] [PubMed]
63. Dai, D.; Qiu, J.; Li, M.; Xu, J.; Zhang, L.; Yao, J. Construction of two-dimensional BiOI on carboxyl-rich MIL-121 for visible-light photocatalytic degradation of tetracycline. *J. Alloy. Compd.* **2021**, *872*, 159711. [CrossRef]
64. Qiu, H.; Zhang, R.; Yu, Y.; Shen, R.; Gao, H. BiOI-on-SiO<sub>2</sub> microspheres: A floating photocatalyst for degradation of diesel oil and dye wastewater. *Sci. Total Environ.* **2020**, *706*, 136043. [CrossRef] [PubMed]
65. Intaphong, P.; Phuruangrat, A.; Thongtem, S.; Thongtem, T. Sonochemical synthesis and characterization of BiOI nanoplates for using as visible-light-driven photocatalyst. *Mater. Lett.* **2018**, *213*, 88–91. [CrossRef]
66. Dayana, P.N.; Abel, M.J.; Inbaraj, P.; Sivarajanji, S.; Thiruneelakandan, R.; Prince, J.J. Zirconium Doped Copper Ferrite (CuFe<sub>2</sub>O<sub>4</sub>) Nanoparticles for the Enhancement of Visible Light-Responsive Photocatalytic Degradation of Rose Bengal and Indigo Carmine Dyes. *J. Clust. Sci.* **2021**, *1*–11. [CrossRef]
67. Ray, S.K.; Dhakal, D.; Lee, S.W. Visible light driven Ni-BaMo<sub>3</sub>O<sub>10</sub> photocatalyst for indigo carmine degradation: Mechanism and pathways. *Mater. Sci. Semicond. Process.* **2020**, *105*, 104697. [CrossRef]
68. Ramos, R.O.; Albuquerque, M.V.; Lopes, W.S.; Sousa, J.T.; Leite, V.D. Degradation of indigo carmine by photo-Fenton, Fenton, H<sub>2</sub>O<sub>2</sub>/UV-C and direct UV-C: Comparison of pathways, products and kinetics. *J. Water Process Eng.* **2020**, *37*, 101535. [CrossRef]